Chemical Engineering Journal 159 (2010) 107–115

Contents lists available at ScienceDirect

Chemical Engineering Journal

journal homepage: www.elsevier.com/locate/cej

Mercury removal from aqueous solutions using silica, polyacrylamide and hybrid silica–polyacrylamide aerogels

Hiba Ramadan[a], Aline Ghanem[b], Houssam El-Rassy[a,*]

[a] Department of Chemistry, American University of Beirut, P.O. Box 11-0236, Riad El-Solh 1107 2020, Beirut, Lebanon
[b] Department of Chemistry, Lebanese University, Faculty of Sciences II, P.O. Box 90-656 Jdeidet El-Matn, Lebanon

ARTICLE INFO

Article history:
Received 26 October 2009
Received in revised form 22 February 2010
Accepted 23 February 2010

Keywords:
Silica
Polyacrylamide
Aerogel
Hybrid
Adsorption
Mercury

ABSTRACT

Mercury(II) ions adsorption from aqueous solutions onto silica, polyacrylamide, and hybrid silica–polyacrylamide aerogels is studied. The aerogels structure was verified by FTIR spectroscopy and their texture by nitrogen adsorption. The adsorbents were tested under different experimental conditions where the effect of temperature, pH, contact time, initial mercury(II) concentration, and aerogels quantity were investigated. The mercury adsorption onto the three aerogels was shown to be very fast, with the fastest being performed at 45 °C onto the hybrid aerogels. pH 11 was revealed optimum indicating a superlative surface interaction between the adsorbent and the adsorbate. The adsorption kinetics follows a pseudo second-order pointing out the co-existence of chemisorption and physisorption with the intra-particle diffusion being the rate controlling step. The mercury(II) adsorption fits well with Langmuir adsorption isotherms where the polyacrylamide aerogels showed the highest adsorption capacity, followed by the hybrid aerogels. The regeneration of the aerogels at pH 2 and their reuse at pH 11 was conducted for three consecutive reuses where the adsorption capacity was successfully maintained. The hybrid aerogels were found to be the most economically interesting adsorbents due to their noticeable adsorptive capacity after regeneration coupled with their no-swelling behavior.

1. Introduction

The existence of heavy metals in wastewaters contributes to water toxicity and represents an increasing danger for the environment, human beings and other living organisms [1,2]. In addition to rock leaching due to some external effects [3], these effluents discharge from various anthropogenic sources such as power plants, chemical manufacturing, painting, mining, metallurgy, electroplating and many other industries [4–6]. Mercury, which is not biodegradable, has been classified by the United States Environmental Protection Agency (EPA) as a high pollutant [7] with a maximum contaminant level of 2 ppb in drinking water. When mercury enters water, some biological processes convert it to methylmercury, which is highly toxic and accumulates in fish, in animals that eat fish, and in predators that eat fish-eating animals [8]. Depending on the level of exposure, the effects of mercury exposure can include alteration of the endocrine system, reduced fertility, slower growth and development, and abnormal behavior that affects survival [9,10]. Thus, the removal of these toxic metals from wastewater is a crucial issue from the environment and health point of view. Several techniques for the removal of mercury ions from wastewaters have been developed such as reduction [11], chemical precipitation [12], membrane separation [13], ion-exchange [14], solvent extraction [15], coagulation [16], and adsorption [17–19]. Among these treatment methods, the mercury adsorption process at the solid-liquid interface was found to be a promising and powerful practice with several advantages: (i) its high efficiency and easiness [20], (ii) its low cost [21] and (iii) the availability of a broad range of adsorbents such as fly ash [22], activated carbon [23], carbon aerogel [24], clay [25], silica surface [26], mesoporous SBA-15 [27], microporous titanosilicate [28] and aluminosilicates [29], polyacrylamide grafted resins [30] and many other adsorbents. Non-toxic hydrophilic cross-linked polyacrylamide hydrogels were found to be high potential adsorbents for toxic metals [31–33]. However, one disadvantage of these superadsorbents from an industrial point of view is their swelling property and therefore the expansion of their networks volume. Thus was the idea of this work to entrap the polyacrylamide network within a hard highly porous inorganic matrix to mechanically control the swelling without affecting the adsorptive capacity of the polyacrylamide polymer. Silica aerogel has been chosen for this purpose. Silica aerogels obtained through the low-temperature sol–gel process [34] and dried under supercritical conditions [35] are highly porous solids showing large specific surface areas (up to 1000 m^2/g), an extraordinarily large surface-to-volume ratio ($\sim 2 \times 10^9\ m^{-1}$) and low densities (0.003–0.35 g/cm^3) [36–38]. Due

* Corresponding author. Tel.: +961 1 350000x3970; fax: +961 1 365217.
E-mail address: Houssam.Rassy@aub.edu.lb (H. El-Rassy).

1385-8947/$ – see front matter © 2010 Elsevier B.V. All rights reserved.
doi:10.1016/j.cej.2010.02.051

to their surface properties as well as the chemical reactivity of their surface groups, these materials deserve a particular interest.

In this study we investigate for the first time the adsorption of mercury ions from aqueous solutions onto porous silica, polyacrylamide, and hybrid silica–polyacrylamide aerogels. The adsorption kinetics and thermodynamics were investigated under different conditions and the adsorption equilibria were studied to determine the best fitting isotherm model to the collected experimental data. The effects of the mercury ions concentration, temperature, pH and adsorbent dosage were studied to determine the optimal adsorption conditions.

2. Experimental

2.1. Materials

The chemicals were used in this study as received and without further purification. Tetramethoxysilane ($Si(OCH_3)_4$; noted TMOS) and Mercury(II) bromide ($HgBr_2$, M.W. 360.40 g/mol) were provided from Merck. Acrylamide and N,N′-methylenebisacrylamide (noted bis-acrylamide) were purchased from Fluka. 2,2-Dimethoxy-2-phenylacetophenone (noted DMPA) was provided by Aldrich. Methanol, hydrochloric acid, and ammonium hydroxide were from Riedel-de-Haen, Panreac and Fischer Scientific, respectively. Double deionized water was prepared in our laboratory.

2.2. Adsorbents synthesis

Polyacrylamide hydrogels were prepared using acrylamide and bis-acrylamide monomers, where the latter was used as a cross-linker allowing the formation of a three-dimensional network. Polyacrylamide hydrogels were prepared in polypropylene vials by mixing 675 μL of a 20% acrylamide solution (w/w), 600 μL of a 2.5% bis-acrylamide solution (w/w) and 1.725 mL of water. To this mixture, 12 μL of a 20% DMPA in methanol (w/w) solution were added. DMPA is used as a photo-initiator. The obtained solution was left for photo-polymerization and aging under UV light (8 W, λ = 302 nm). After 1 h, clear polyacrylamide hydrogels were obtained, containing 5% monomers (w/w) with an acrylamide:bis-acrylamide ratio equal to 9:1.

Silica alcogels were synthesized through a two-step sol–gel process. In the first step, TMOS was mixed in polypropylene vials with methanol, hydrochloric acid solution (0.2 M) and deionized water for 24 h. An ammonium hydroxide solution (0.5 M) was then added to the solution and mixed together for 1 min. The gelation of the sols was observed in the next 30 min and obtained alcogels were kept for aging for 2 h at room temperature. The final molar ratio TMOS:Methanol:H_2O:HCl:NH_3 was 1:11.9:6: 3×10^{-3}:6×10^{-3}.

To prepare the hybrid solid, silica alcogels prepared according to the previously mentioned procedure were dipped in double distilled water for 24 h to insure the complete exchange of the liquids filling the pores with water. The wet silica gels were then transferred to a flask containing an acrylamide/bis-acrylamide/DMPA solution. This latter solution was identical to the one used in the preparation of the polyacrylamide hydrogels. It is worth to mention that the organic monomers solution's volume was 20 times larger than that of the silica gel to allow the best exchange of water filling the silica network pores with the organic monomers solution. After 24 h of exchange, silica gels soaked with acrylamide/bis-acrylamide monomers were left for 1 h under UV light (8 W, λ = 302 nm) to accomplish the photo-polymerization of the acrylamide and bis-acrylamide within the silica pores and to lead to the hybrid silica–polyacrylamide wet gel.

The silica alcogel, polyacrylamide hydrogel and hybrid silica–polyacrylamide wet gel were soaked in acetone for 24 h before being dried under supercritical carbon dioxide (T_c = 31.1 °C; P_c = 73.7 bar). Acetone was used as an intermediate solvent presenting a higher miscibility with liquid carbon dioxide than water and methanol. This drying technique led to the formation of the so-called silica, polyacrylamide and hybrid silica–polyacrylamide aerogels.

2.3. Adsorbents characterization

A complete structural, textural and morphological characterization of these aerogels was performed [39], however we opt to present here only three of the used techniques. The surface properties of the three adsorbents were determined by using the nitrogen adsorption–desorption technique. N_2 isotherms were measured at 77 K using a Nova 2200e high-speed surface area and pore size analyzer (Quantachrome Instruments) after degassing the samples for 2 h at 120 °C. The specific surface area was reported according to the BET theory [40] while the pore size and pore volume were calculated by the BJH method [41]. The particle size distribution was determined by optical microscopy using an Axiovert 200 Carl Zeiss Inverted Microscope. The infrared spectroscopy measurements were performed on a Thermo Nicolet 4700 Fourier Transform Infrared Spectrometer equipped with a Class 1 Laser using the transmission KBr pellet technique, where 1% in weight aerogel powder-containing potassium bromide pellets were used.

2.4. Adsorption studies

Adsorption experiments were performed at 30, 45, or 60 °C in glass vials placed in a controlled-temperature shaking water bath operating at 200 rpm. In typical adsorption experiments, 100 mg of silica, polyacrylamide or hybrid silica–acrylamide aerogel were added to 15 mL of a mercury(II) bromide aqueous solution. Unless specified otherwise, the mercury concentration was 50 ppm ($[Hg^{2+}]$ = 50 mg/L). Aliquots were taken from the solution at predetermined time intervals and centrifuged for 15 min at 4300 rpm ($3866 \times g$) using a Heraeus Megafuge 1.0R equipped with a Heraeus 2704 swing-out rotor. The concentration of Hg(II) was determined by Atomic Absorption Spectrometry (AAS) using a Thermo Elemental Solaar M6 Atomic Absorption Spectrometer using a hollow cathode lamp at λ = 253.7 nm and equipped with a CETAC ASX-510 autosampler. According to the IUPAC method [42], the mercury detection limit was experimentally determined and found to be 4 ppm. The amount of mercury(II) ions adsorbed on the aerogels was calculated according to the following equation:

$$q_e = \frac{(C_i - C_e)}{m} V \quad (1)$$

where q_e is the quantity of mercury adsorbed (mg/g), C_i and C_e are the initial and equilibrium liquid-phase concentrations of mercury (mg/L), respectively, V is the volume of the solution (L) and m is the quantity of adsorbent used (g).

The effect of pH was studied after the adjustment of the solutions pH between 2 and 11 using dilute HCl or NaOH solutions; A Corning Pinnacle 542 pH conductivity meter with a combined pH electrode was used for this purpose. The initial mercury(II) concentration was studied between 30 and 300 mg/L, the dosage of the adsorbent was studied in the 20–500 mg range, and the activity of regenerated adsorbents was examined after successive cycles.

3. Results and discussion

3.1. Adsorbents characterization

The nitrogen adsorption–desorption isotherms of the three aerogels (not shown) revealed large differences in the specific surface area (SSA), pore volume (V_p), and pore size distribution. Hybrid and silica aerogels revealed type IV isotherms as indicated by the IUPAC classification of sorption isotherms [43]. It was noticed that the existence of the polyacrylamide network reduced the SSA of the hybrid aerogel to 572 m^2/g compared to the silica aerogel having a SSA equal to 623 m^2/g. Moreover, the pore volume increased from 1.49 cm^3/g for the silica aerogel to 1.92 cm^3/g for the hybrid aerogel. We can conclude that the hybrid aerogel profits from the existence of the organic polymer to reduce its shrinkage during the supercritical drying and thus larger pore volumes are obtained. The N_2 isotherms performed on the polyacrylamide aerogel showed a mesoporous material with low specific surface area (40 m^2/g) and pore volume (0.04 cm^3/g).

The particle size measurements show a very broad spectrum of sizes for each aerogel. Silica aerogel particles range between 5 and 50 μm, polyacrylamide aerogel particles are between 30 and 100 μm and hybrid aerogels particles range between 5 and 100 μm.

The FTIR spectra of the silica, polyacrylamide and hybrid silica–polyacrylamide aerogels (not shown) reveal bands that correspond to the solid networks structural units. In addition to the bands appearing at 3450 and 1635 cm^{-1} corresponding respectively to the adsorbed water and surface silanol groups [34,44], the silica aerogel exhibits bands at 1200–1080 and 801 cm^{-1} easily attributed to the Si–O–Si asymmetric and symmetric stretching vibrations of the silica network respectively [34,45]. Besides, the infrared spectrum of the silica aerogel shows a weak C–H symmetric deformation peak at 1384 cm^{-1} that corresponds to residual non-hydrolyzed methoxy groups on the surface of the gel [46]. On the other hand, the polyacrylamide aerogel spectrum shows bands between 2970 and 2700 cm^{-1} attributed to the C–H symmetric and asymmetric stretching vibrations respectively and a band at 1450 cm^{-1} attributed to the C–H deformation vibration [46]. The spectrum reveals also bands at 1668 and 1536 cm^{-1} assigned to the C=O [47] and N–H [48] bending modes, respectively. The FTIR spectrum of the hybrid aerogel shows bands at 1200–1050 cm^{-1} and 960 cm^{-1} characteristic of the silica network as well as bands at 1669 cm^{-1}, 1536 cm^{-1} and 1450 cm^{-1} corresponding to the polyacrylamide network. These peaks confirm the co-existence in the hybrid aerogel of the silica and polyacrylamide networks.

3.2. Effect of pH on adsorption

The effect of pH on the adsorption of mercury(II) ions on the three aerogels was studied in the pH range between 2 and 11. For that purpose, 100 mg of aerogel powder were added to a 50 mg/L mercury solution where the pH was adjusted using dilute HCl or NaOH solutions. The experiments were conducted at 30 °C. The AAS measurements done after 24 h showed the maximum adsorption for the three aerogels to be at pH 11 with a considerable increase of the adsorption capacity of the aerogels at pH values greater than 9 (Fig. 1). It is worth to note that the adsorption capacities for the three aerogels were roughly identical at pH 11. In the other hand, the silica and hybrid aerogels did not show any adsorption at pH 2 and 3, and the polyacrylamide aerogel did not adsorb mercury ions when the pH was smaller than 5. The silica aerogel showed the weakest adsorption being approximately constant (not exceeding 14%) for a pH smaller than 9; however, the polyacrylamide aerogel showed a gradual increase in the adsorption capacity in the same pH range. The hybrid aerogel revealed an adsorption capacity slightly greater than the polyacrylamide at pH smaller than 8 and slightly weaker at larger pH values. The difference in the adsorption capacity is mainly due to the adsorbent surface charge. As silica has a point of zero charge around 2.5 [49], the adsorbent exhibits a positive zeta potential at pH lower than this value. Therefore, the surface will be positively charged at this pH which reduces the adsorption due to the electrostatic repulsion between the surface and the mercury cations. In the other side, the adsorption increases as the pH increases due to the increase of the silica surface negative charges favoring the electrostatic attraction between the two entities with opposite charges, $Si–O^-$ and Hg^{2+}. The polyacrylamide aerogel is made of successive and cross-linked units of acrylamide and bis-acrylamide and thus has some pH-sensitive $CONH_2$ surface groups. At low pH, these groups are protonated and result in repulsion with the mercury cations minimizing the adsorption capacity of the aerogel. However, at high pH the adsorption is favored. The hybrid aerogel has a high adsorption capacity comparable to the silica and polyacrylamide networks, as both networks, the inorganic and organic, show identical adsorption trends when the pH changes.

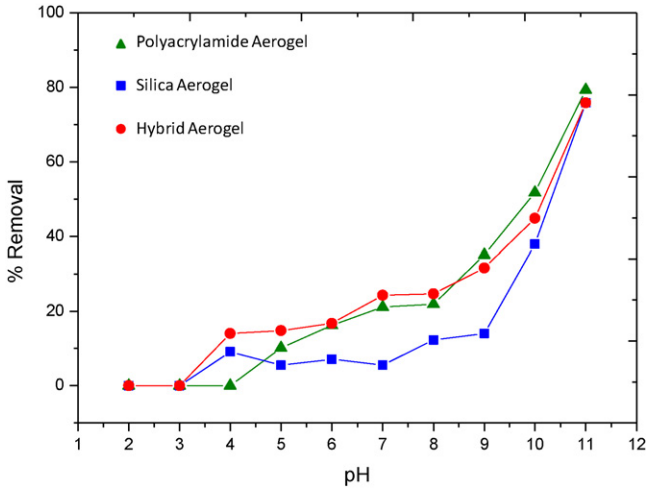

Fig. 1. Effect of pH on adsorption of mercury(II) ions. Initial mercury(II) concentration = 50 mg/L; contact time = 24 h; mass of adsorbent = 100 mg; solution volume = 15 mL.

3.3. Effect of contact time

The effect of contact time was studied for the three aerogels with 50 ppm mercury(II) solution. For that purpose 2 g of each aerogel were used and the experiments were performed in 300 mL of mercury solution at 30, 45, and 60 °C with the pH being adjusted to 11. The large volume of solution used in these experiments allowed us to take a large number of aliquots without affecting the results. It is worth to note that the solid to mercury ratio used in this section is the same as in the other parts of this study where 100 mg of adsorbents and 15 mL of solution were used. The AAS measurements, carried out for various aliquots withdrawn from the solutions at different time intervals over the first 30 min of contact time, showed a very fast adsorption of mercury(II) ions on the three solids with the hybrid aerogel being the material showing the highest adsorption initial rate (Fig. 2). Hybrid aerogels show a very high efficiency where their uptake exceeds 50% of the mercury ions existing in the solution during the first 90 s, with the adsorption at 45 °C being the fastest. It was also noticed that the silica aerogel adsorption capacity decreases when the temperature increases. However, the adsorption onto the polyacrylamide aerogel appeared slower for the experiment done at 45 °C compared to those at 30 and 60 °C during the first minutes, with the quantity adsorbed after 30 min

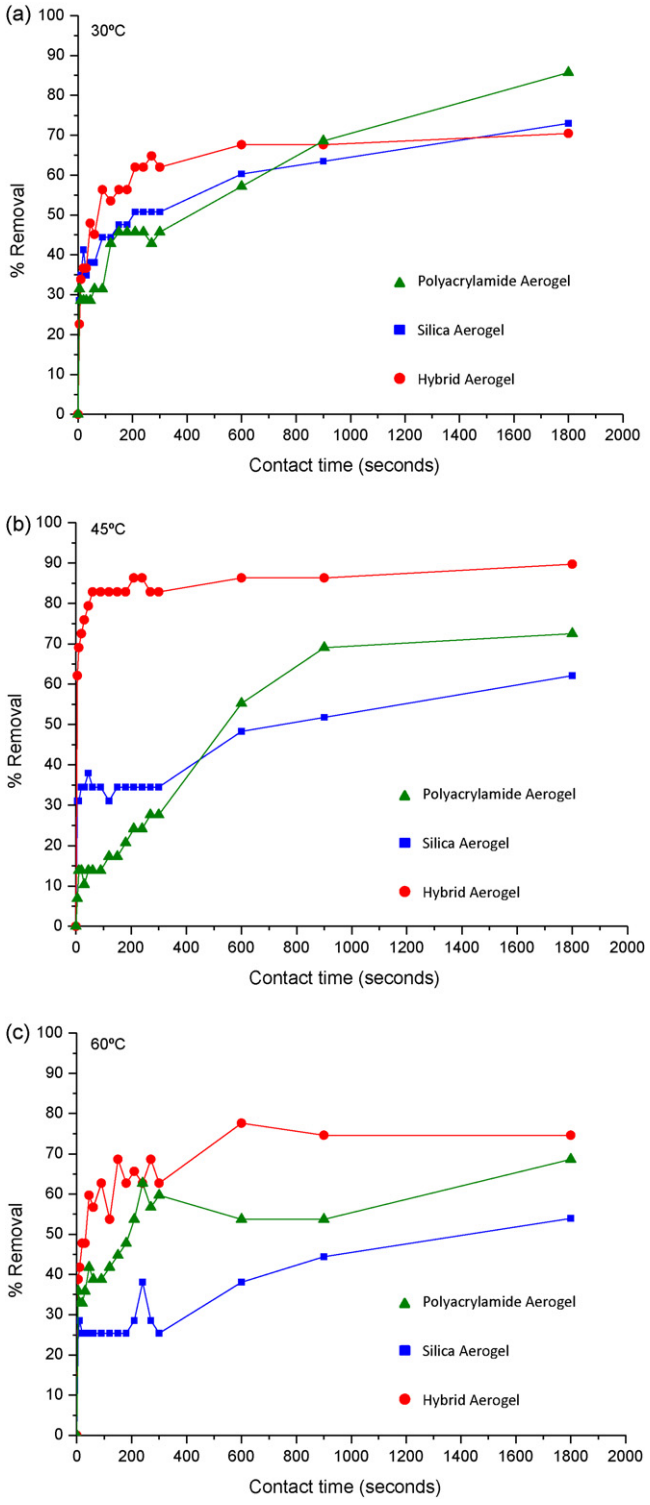

Fig. 2. Evolution of adsorbed quantity of mercury(II) with time. $[Hg^{2+}]_0 = 50$ mg/L; mass of adsorbent = 2 g; solution volume = 300 mL; pH = 11. Adsorption tests performed at 30 °C (a), 45 °C (b), and 60 °C (c).

being inversely proportional to the temperature. The differences in the adsorption capacity at various temperatures seem not to be only dependent on the adsorption equilibrium constants. To guarantee the maximum adsorption on the aerogels and a complete equilibrium condition, the subsequent experiments were performed with 24 h contact time.

3.4. Effect of initial mercury(II) concentration

The mercury(II) adsorption capacity of the three aerogels has been studied as a function of the metal initial concentration. The mercury(II) ion concentration was between 30 and 300 mg/L, the pH of the solutions was adjusted to 11, the experiments were performed at 30, 45, and 60 °C, and the mercury concentrations were measured after 24 h of contact. As the studied mercury(II) concentrations were far below the mercury(II) bromide solubility which is 6.1 g/L at 25 °C, the decrease in the mercury(II) concentration is due to its adsorption on the surface of the aerogel and not to the recrystallization of the mercury salt. Fig. 3 shows the change in the percent removal and q_e as a function of the mercury(II) concentration. It was noticed that polyacrylamide and silica aerogels have the greatest and the weakest adsorption capacities respectively, regardless the experiment temperature. The polyacrylamide aerogels showed comparable adsorption behavior at 30 and 60 °C, where

q_e reaches around 12–13 mg/g for mercury(II) concentrations near 300 mg/L. However, the experiment performed at 45 °C showed a different adsorption trend, where the plot of q_e versus mercury concentration revealed a continuous increase as the mercury concentration increases. q_e almost 16 mg/g was obtained when the mercury concentration was 300 mg/L. Moreover, silica aerogels exhibited lower adsorption capacities compared to the polyacrylamide and hybrid aerogels. The largest q_e calculated for the silica aerogels was approximately 11 mg/g at 45 °C. As for the polyacrylamide and silica aerogels, hybrid aerogels showed the best adsorption capacity at 45 °C with q_e reaching 13 mg/g, however the values were 12 and 8 mg/g for the experiments performed at 30 and 60 °C, respectively. The observed similarity between polyacrylamide and hybrid aerogels, revealing comparable adsorption trends with the latter being less active, is an excellent proof that the silica network in the hybrid aerogel is not affecting the adsorption capacity of the acrylamide polymer. The organic network performs in the same way as if it was alone, and the difference in q_e is mainly due to the fact that the hybrid aerogel has a certain percentage of its mass being organic (polyacrylamide) and the remaining is inorganic (silica).

3.5. Effect of adsorbent dose

To investigate the effect of the various aerogels dosage on the adsorption capacities, several quantities of these adsorbents were tested where masses between 20 and 500 mg were used per experiment. The experiments were performed at 30, 45, and 60 °C in 15 mL aqueous solutions containing 50 mg/L of mercury(II) with the pH being adjusted to 11. The AAS measurements done after 24 h showed that the best adsorption was observed for the experiments carried out at 45 °C regardless the quantity of adsorbent used (Fig. 4). In addition, a difference in the amount of mercury(II) adsorbed was clear especially when the mass of the adsorbent was below 100 mg. Conversely, a weaker difference was observed for larger quantities of adsorbent. We noticed that 20 mg of polyacrylamide aerogel were able to adsorb 82% (31.5 mg/g) of the quantity of mercury in the solution while a similar mass of silica or hybrid aerogels were not able to adsorb more than 47% (18.1 mg/g) and 63% (24.2 mg/g) of the initial mercury(II) ions, respectively. The plots of $1/q_e$ versus the mass of the adsorbent, shown for the three adsorbents used at various temperatures, bare excellent linear trends ($0.9999 > R^2 > 0.9934$) that point out the availability of the adsorption sites when large adsorbent quantities are tested as well as if very small quantities are used.

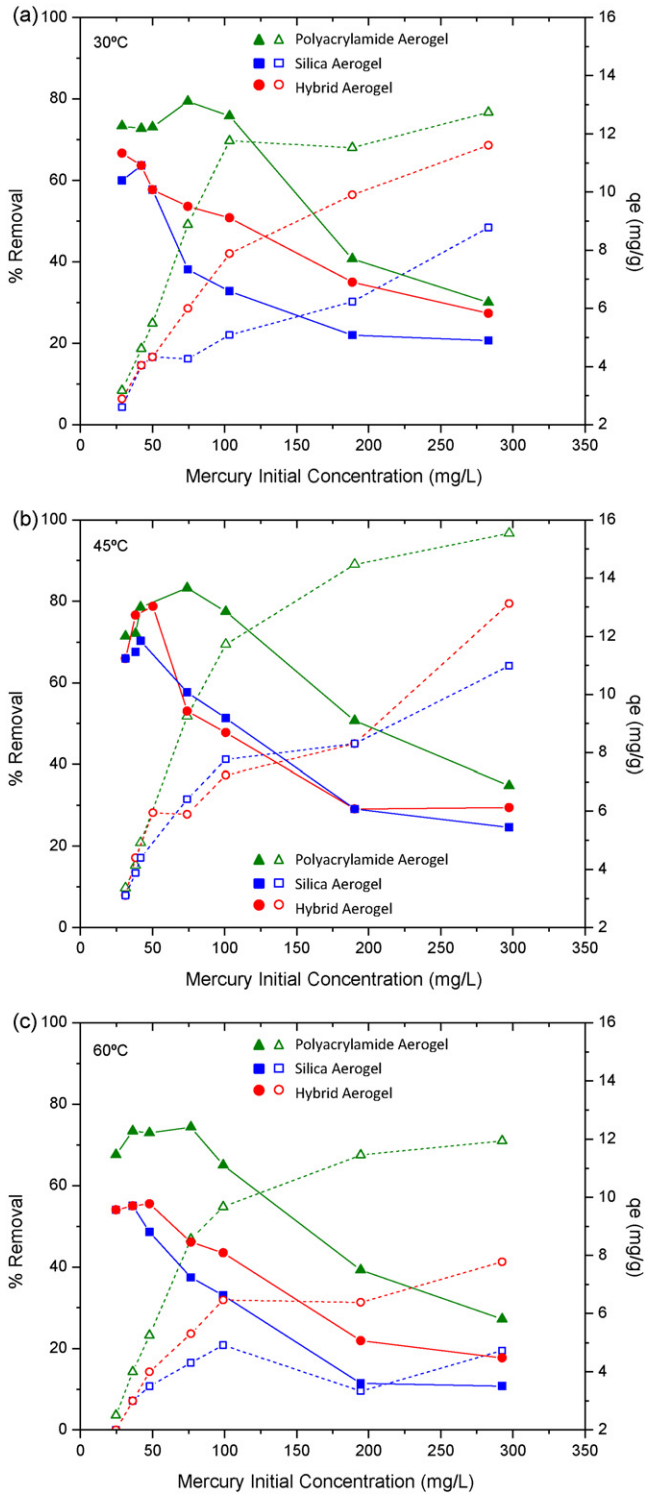

Fig. 3. Effect of initial mercury(II) concentration on adsorption. $[Hg^{2+}]_0$ = 30–300 mg/L; contact time = 24 h; mass of adsorbent = 100 mg; solution volume = 15 mL; pH = 11. Adsorption tests performed at 30 °C (a), 45 °C (b), and 60 °C (c).

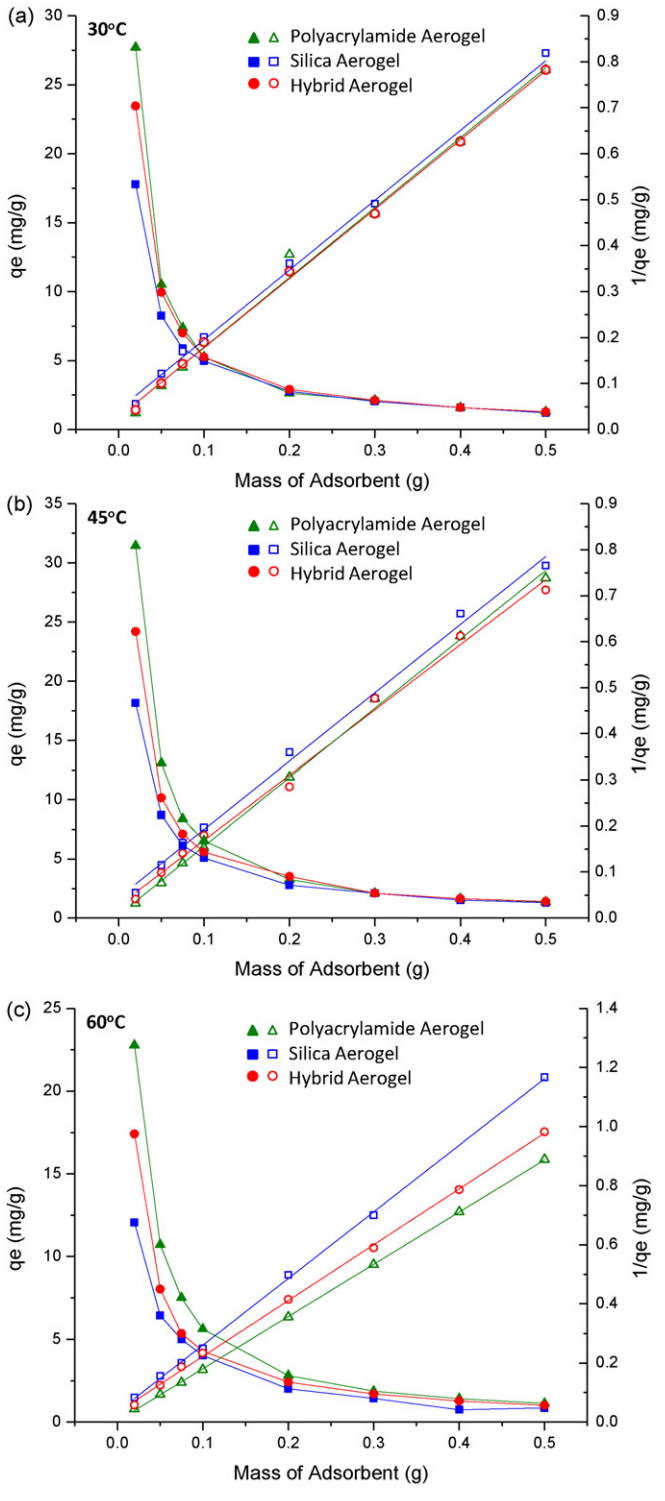

Fig. 4. Influence of adsorbent dose on mercury(II) adsorption after 24 h. $[Hg^{2+}]_0$ = 50 mg/L; contact time = 24 h; solution volume = 15 mL; pH = 11. Adsorption tests performed at 30 °C (a), 45 °C (b), and 60 °C (c).

3.6. Mercury adsorption isotherms

Collected adsorption data at mercury(II) concentrations ranging between 30 and 300 mg/L at various temperatures were fitted with four common adsorption models: Langmuir [50], Freundlich [51], Temkin [52], and Dubinin–Radushkevich [53] isotherm models.

The Langmuir isotherm equation is represented by

$$q_e = \frac{q_{max} K_L C_e}{1 + K_L C_e} \quad (2)$$

where q_{max} is the monolayer capacity of the adsorbent (mg/g) and K_L is the Langmuir equilibrium constant (L/mg). By using the linear form of this isotherm, the plot of C_e/q_e versus C_e gives a line with a slope of $1/q_{max}$ and an intercept of $1/K_L q_{max}$.

Table 1
Langmuir, Freundlich, Temkin and Dubinin–Radushkevich isotherms coefficients for adsorption of mercury(II) bromide onto polyacrylamide, silica, and hybrid silica–polyacrylamide aerogels.

	Langmuir isotherm			Freundlich isotherm			Temkin isotherm			Dubinin–Radushkevich isotherm			
	q_{max} (mg/g)	K_L (L/mg)	R^2	n	K_F (L/g)	R^2	b_T (MJ/mol)	K_T (L/g)	R^2	β (mol^2/J^2)	q_{max} (mg/g)	E (kJ/mol)	R^2
Polyacrylamide aerogel													
30 °C	13.75	5.90×10^{-2}	0.988	2.802	6.11×10^{-4}	0.655	339.1	2.98×10^{5}	0.723	3.17×10^{-9}	46.84	12.60	0.687
45 °C	17.63	4.23×10^{-2}	0.979	2.346	1.30×10^{-3}	0.708	257.0	1.74×10^{5}	0.836	3.39×10^{-9}	71.69	12.14	0.731
60 °C	13.21	4.99×10^{-2}	0.990	2.467	8.47×10^{-4}	0.750	363.3	2.00×10^{5}	0.872	2.98×10^{-9}	52.35	12.95	0.784
Silica aerogel													
30 °C	9.17	2.68×10^{-2}	0.930	3.228	2.12×10^{-4}	0.859	570.0	1.88×10^{5}	0.839	2.73×10^{-9}	19.58	13.53	0.852
45 °C	11.60	3.68×10^{-2}	0.976	2.794	4.41×10^{-4}	0.909	423.3	1.73×10^{5}	0.950	2.87×10^{-9}	33.17	13.20	0.924
60 °C	4.42	1.14×10^{-2}	0.944	5.429	5.07×10^{-5}	0.480	1655.1	3.32×10^{6}	0.468	1.42×10^{-9}	8.50	18.76	0.517
Hybrid aerogel													
30 °C	13.69	5.90×10^{-2}	0.996	2.206	1.04×10^{-3}	0.969	311.0	9.04×10^{4}	0.989	4.00×10^{-9}	50.96	11.18	0.981
45 °C	13.19	5.90×10^{-2}	0.900	3.139	3.33×10^{-4}	0.786	422.8	2.22×10^{5}	0.790	2.48×10^{-9}	28.49	14.20	0.775
60 °C	8.39	5.90×10^{-2}	0.985	2.586	4.11×10^{-4}	0.827	576.6	1.46×10^{5}	0.906	2.91×10^{-9}	28.48	13.11	0.858

The empirical equation used to describe the Freundlich isotherm is given by

$$q_e = K_F C_e^{1/n} \tag{3}$$

where n is the heterogeneity factor and K_F is the Freundlich constant (L/g), both commonly temperature dependent. n is typically greater than 1 and the larger is its value, the adsorption isotherm becomes more non-linear and the system becomes more heterogeneous [54]. The linearized form of the Freundlich equation allows the determination of n and K_F from a linear plot of $\ln q_e$ versus $\ln C_e$.

The Temkin isotherm equation is represented by

$$q_e = \frac{RT}{b_T} \ln C_e + \frac{RT}{b_T} \ln K_T \tag{4}$$

where R is the gas constant (8.3145 J/mol K), T is the absolute temperature, b_T is the variation of the adsorption energy (J/mol), and K_T is the equilibrium binding constant (L/g). Accordingly, the plot of q_e versus $\ln C_e$ gives a linear plot allowing the determination of b_T and K_T.

The Dubinin–Radushkevich (D–R) isotherm is analogous to the Langmuir isotherm without assuming a homogeneous surface or constant sorption potential. This isotherm is represented by

$$q_e = q_{max} \ \exp(-\beta\varepsilon^2) \tag{5}$$

where q_{max} is the D–R monolayer capacity (mol/g), β is a constant related to the adsorption energy (mol^2/kJ^2), and ε is the Polanyi potential related to the equilibrium concentration as follows:

$$\varepsilon = RT \ \ln\left(1 + \frac{1}{C_e}\right) \tag{6}$$

The plot of $\ln q_e$ versus $\ln^2(1 + 1/C_e)$ reveals a linear plot allowing the determination of β and q_{max}. The mean free energy of adsorption, E (J/mol), can be calculated according to the following relationship:

$$E = \frac{1}{\sqrt{2\beta}} \tag{7}$$

The Langmuir, Freundlich, Temkin and Dubinin–Radushkevich isotherm constants were computed from the linear isotherm graphs for each of the isotherm equations tested. These constants as well as the coefficients of determination (R^2) are regrouped in Table 1. After comparing the four theoretical models to the experimental data, it was obviously found that the Langmuir isotherm represents the best fit of the experimental results over the other isotherms. Theoretically calculated maximum monolayer capacities (q_{max}) from the Langmuir model were found to be the best for the experiments carried out at 45 °C when compared to the values found at 30 and 60 °C, except for the hybrid aerogel where the values obtained at 30 and 45 °C were found very similar. Calculated q_{max} values from the fit are 17.63, 11.60 and 13.19 mg/g for the polyacrylamide, silica, and hybrid aerogels at 45 °C, respectively. These values are highly comparable to those mentioned previously in Section 3.5 and experimentally obtained when high concentrations of mercury(II) were used.

3.7. Adsorption kinetics

Experimental data obtained at various contact time over the first 30 min of the experiment were used for the investigation of the adsorption kinetics at 30, 45 and 60 °C and compared to theoretical models. For that purpose, pseudo first-order and pseudo second-order kinetic models were tested.

The pseudo first-order equation is

$$\ln(q_e - q_t) = \ln \ q_e - k_1 t \tag{8}$$

And the pseudo second-order equation is

$$\frac{t}{q_t} = \frac{t}{q_e} + \frac{1}{k_2 q_e^2} \tag{9}$$

where q_e and q_t are the adsorption capacity of the solid material at equilibrium (mg/g) and the quantity of mercury(II) adsorbed at time t (mg/g), respectively. k_1 (s^{-1}) and k_2 (g/mg s) are the corresponding rate constants.

Fitting the obtained data with these two models shows that the pseudo second-order kinetic model is the best matching, with the superlative fit appears for the hybrid aerogels at the three tested temperatures. The plots of t/q_t versus t reveal a perfect linearity as shown in Fig. 5. Calculated k_2 values are 6.16×10^{-3}, 1.55×10^{-2}, and 7.28×10^{-3} g/mg s for the experiments performed at 30, 45, and 60 °C, respectively. These values reveal one more time that the adsorption is the fastest at 45 °C. This model suggests that the mercury(II) adsorption depends on the adsorbate as well as the adsorbent and that a chemisorption process is involved in this sorption in addition to physisorption. The former might be the rate limiting step where valency forces are involved via electrons sharing or exchange between the aerogel and the mercury ions [55].

3.8. Adsorption mechanism

Four steps are involved in the adsorption process of metal ions from aqueous solutions onto the surface of solid materials. These steps are (i) the transport of the ions within the solution; (ii) their external diffusion or boundary layer diffusion, which is the diffusion through the liquid film neighboring the solid particle; (iii) the diffusion within the liquid incorporated in the pore, known by internal diffusion or intra-particle diffusion; (iv) the adsorption or desorption on the surface of the interior adsorption sites [56].

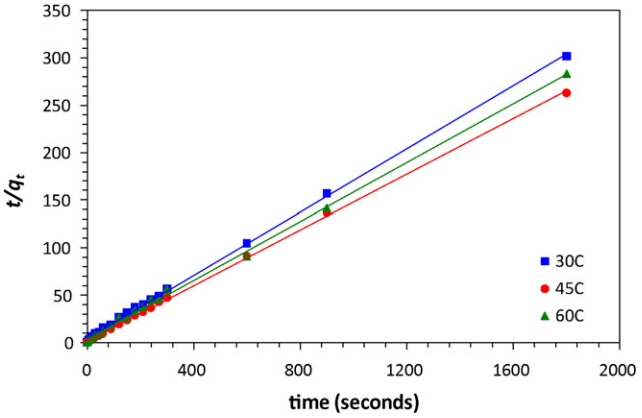

Fig. 5. Pseudo second-order kinetic plots for adsorption of mercury(II) ions on hybrid silica–polyacrylamide aerogels. $[Hg^{2+}]_0 = 50$ mg/L; mass of adsorbent = 100 mg; solution volume = 15 mL; pH = 11.

As the experiments are performed under fast shaking, the transport of the ions within the solution is rapid and therefore the first step could not be the rate limiting step in the adsorption process. Besides, the adsorption/desorption step on the surface (step 4) is known to be fast [57], which makes the boundary layer diffusion or the intra-particle diffusion to be the rate controlling factors. It was shown that, if the adsorption process is influenced by the intra-particle diffusion, the uptake of the mercury(II) ions q_t should vary linearly with the square root of time t [58]. This dependence is expressed as follows:

$$q_t = k_{ipd}\ t^{0.5} + C \tag{10}$$

where k_{ipd} is the intra-particle diffusion rate constant (mg/g $s^{0.5}$) and C is the intercept.

Plotting the collected data for the three aerogels at 30, 45 and 60 °C revealed non-linear plots over the whole range; nevertheless, a tri-linearity appears reflecting the existence of three successive adsorption steps [59]. An example of this tri-linearity is shown in Fig. 6 where we chose to plot q_t versus $t^{0.5}$ for the hybrid aerogels. Silica and polyacrylamide aerogels exhibited similar behavior. Since the first linearity slope is larger than that of the second, hence the first step, being the external surface adsorption correlated to the boundary layer diffusion, is faster than the second assigned to the intra-particle diffusion. Accordingly, this latter is greatly concerned in the rate control of this mechanism. The last linearity is attributed to the equilibrium stage. By looking at the second linearity, we can easily notice that it does not pass by the origin, which points out

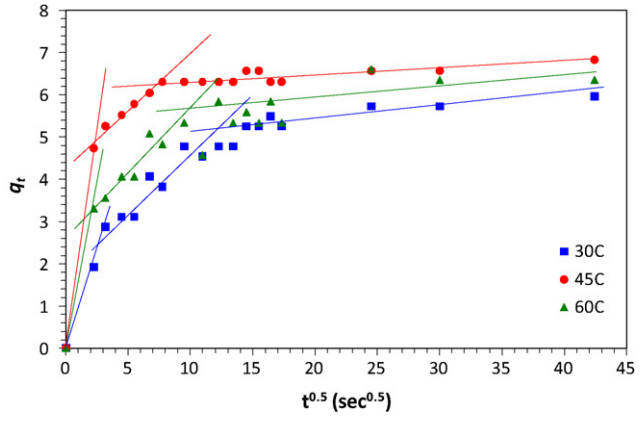

Fig. 6. Intra-particle diffusion plots for adsorption of mercury(II) ions on hybrid silica–polyacrylamide aerogels. $[Hg^{2+}]_0 = 50$ mg/L; mass of adsorbent = 100 mg; solution volume = 15 mL; pH = 11.

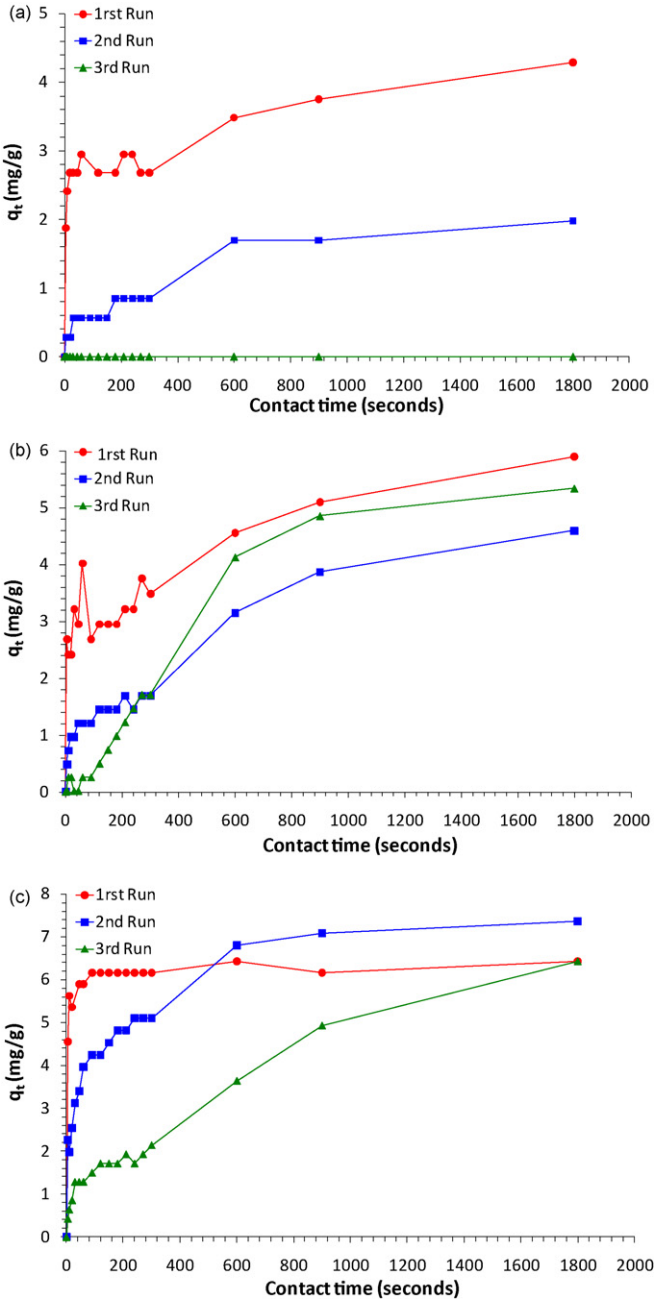

Fig. 7. Effect of consecutive experiments on the adsorption of mercury(II) ions. $[Hg^{2+}]_0 = 50$ mg/L; mass of adsorbent = 2 g; solution volume = 300 mL; pH = 11; $T = 45$ °C. Adsorption tests performed for silica aerogels (a), polyacrylamide aerogels (b), and hybrid silica–polyacrylamide aerogels (c).

that the intra-particle diffusion is involved with other mechanisms in the mercury ions adsorption rate control [59].

3.9. Recovery and reuse of adsorbents

Testing the recovery and the reusability of the adsorbents was done at 45 °C where adsorbed mercury ions at pH 11 (1st run) were desorbed at pH 2. Recovered solids were reused in a second run of adsorption at pH 11 (2nd run) followed by a desorption at pH 2 and an adsorption at pH 11 (3rd run). Adsorption runs were performed at the same conditions as in paragraph 3.3 (2 g of adsorbent and 300 mL of 50 ppm mercury(II)) and desorption was done in water at pH 2. The adsorbents were collected after each step by filtration and left to dry at room temperature for 24 h. We noticed a minor

lost of powder during the filtration process, hence we considered the quantity of powder used in all these steps to be constant (2 g). The pH of desorption was selected according to Section 3.2 where no adsorption was noticed at pH 2 and thus the adsorption of mercury onto the aerogels surface is negligible at this pH, and therefore desorption should be maximal. In this section, the adsorption was followed over the first 30 min of each run and the desorption was followed over 5 h.

The desorption tests showed different behavior for the three used aerogels where the desorption was not complete even after 5 h at pH 2. AAS measurements revealed a plateau at 63.9% of desorption after 1 h for the first desorption, i.e. relative quantity of mercury released in the solution compared to the quantity adsorbed by the solid in the previous adsorption, and at 55.6% after 15 min for the second desorption when silica aerogels were used as adsorbents. Polyacrylamide aerogels showed a plateau at 51.6% of desorption after 90 min for the first desorption and at 56.4% after 30 min for the second desorption. A plateau was seen at 68.5% of desorption after 15 min for the first desorption and at 68.9% after 10 min for the second desorption when hybrid aerogels were the adsorbents. By looking at these values, we can easily notice that the mercury ions were never totally desorbed from the surface of the solids.

Adsorption tests over three runs showed that the aerogels remain active after three runs except for the silica which shows no adsorption at the third run. While comparing to the first run the quantity of mercury adsorbed by weight of adsorbent at 300 s (q_{300}) for the successive runs (2nd and 3rd), we found maintained adsorption capacities equal to (i) 32% in the second run and 0% in the third run for the silica aerogel (ii) 49% in the second run and 49% in the third run for the polyacrylamide aerogel (iii) 83% in the second run and 35% in the third run for the hybrid aerogel. Corresponding plots are shown in Fig. 7.

By comparing and combining these adsorption and desorption results, we found that the hybrid aerogels show the best behavior in adsorption and desorption where the mercury desorption from these materials is the fastest when compared to the two other aerogels. In addition, the quantity adsorbed on the hybrid aerogel after three runs (q_{300} = 2.14 mg/g) is higher than that adsorbed after the second run on the silica aerogel (q_{300} = 0.85 mg/g) and on the polyacrylamide aerogel (q_{300} = 1.69 mg/g).

4. Conclusions

Silica, polyacrylamide, and hybrid silica–polyacrylamide aerogels were used as adsorbents for mercury(II) ions from aqueous solutions and tested under various experimental conditions. The pH is found to be a major parameter affecting the adsorption ability of these aerogels where a pH value equal to 11 was observed to be the optimum, reflecting the best interaction between the mercury ions and the solid surface groups. A very fast adsorption of mercury(II) ions was noticed within the first 90 s of the experiment where, for the three adsorbents, the uptake exceeded 50% of the initial mercury amount in the solution with the hybrid aerogel being the fastest especially at 45 °C. However, the AAS measurements performed after 24 h for all the tests carried out at other conditions showed the polyacrylamide having a higher adsorption capacity. Besides, increasing the concentration of mercury(II) ions showed an increase of the uptake capacity of the three aerogels where the highest adsorption capacity was noted for the polyacrylamide aerogel at 45 °C. The modification of the adsorbent dose revealed a very similar behavior for the polyacrylamide and hybrid aerogels with the polyacrylamide having a higher adsorption capacity. Fitting the experimental data with theoretical models bares a perfect matching with the Langmuir adsorption isotherm model with the theoretical maximum uptake being for the polyacrylamide aerogel at 45 °C (17.63 mg/g). The experiments revealed also an adsorption that follows a pseudo second-order kinetics model indicating the involvement of chemical reactions in addition to physisorption in the adsorption process. Besides being efficient as adsorbents for mercury ions, the aerogels are economically interesting materials as they are found to be reusable for adsorption after regeneration.

In conclusion, this study showed the silica, polyacrylamide and hybrid silica–polyacrylamide aerogels to be highly efficient adsorbing materials for mercury(II) ions, economically attractive, easily regenerated and reusable several times. A special consideration is for the hybrid aerogels that are the most industrially appealing thanks to their high adsorption capacity along with no swelling behavior. This latter is a large limitation for the industrial application of the polyacrylamide aerogels.

Acknowledgments

The authors gratefully acknowledge the American University of Beirut Research Board for the financial support. The authors would like to acknowledge the Central Research Science Lab (CRSL) of the Faculty of Arts and Sciences at AUB where the AAS and optical microscopy were performed.

References

[1] J.O. Nriagu, J.M. Pacyna, Quantitative assessment of worldwide contamination of air, water and soils by trace metals, Nature 333 (1988) 134–139.
[2] G Mance, Pollution Threat of Heavy Metals in Aquatic Environments, Elsevier Applied Science, 1987.
[3] S. Da Pelo, E. Musu, R. Cidu, F. Frau, P. Lattanzi, Release of toxic elements from rocks and mine wastes at the Furtei gold mine (Sardinia, Italy), Journal of Geochemical Exploration 100 (2009) 142–152.
[4] J. Dong, Z. Xu, F. Wang, Engineering and characterization of mesoporous silica-coated magnetic particles for mercury removal from industrial effluents, Applied Surface Science 254 (2008) 3522–3530.
[5] A.K. Meena, G.K. Mishra, P.K. Rai, C. Rajagopal, P.N. Nagar, Removal of heavy metal ions from aqueous solutions using carbon aerogel as an adsorbent, Journal of Hazardous Materials 122 (2005) 161–170.
[6] X.L. Jianjun Xie, Jifu Liang, Absorbency and adsorption of poly(acrylic acid-co-acrylamide) hydrogel, Journal of Applied Polymer Science 106 (2007) 1606–1613.
[7] L. Keith, W. Telliard, ES'T special report: priority pollutants: I-a perspective view, Environmental Science & Technology 13 (1979) 416–423.
[8] L.C. Chasar, B.C. Scudder, A.R. Stewart, A.H. Bell, G.R. Aiken, Mercury cycling in stream ecosystems. 3. Trophic dynamics and methylmercury bioaccumulation, Environmental Science & Technology 43 (2009) 2733–2739.
[9] S.W. Tan, J.C. Meiller, K.R. Mahaffey, The endocrine effects of mercury in humans and wildlife, Critical Reviews in Toxicology 39 (2009) 228–269.
[10] X. Zhu, Y. Kusaka, K. Sato, Q. Zhang, The endocrine disruptive effects of mercury, Environmental Health and Preventive Medicine 4 (2000) 174–183.
[11] A. Oehmen, J. Fradinho, S. Serra, G. Carvalho, J.L. Capelo, S. Velizarov, J.G. Crespo, M.A.M. Reis, The effect of carbon source on the biological reduction of ionic mercury, Journal of Hazardous Materials 165 (2009) 1040–1048.
[12] M.M. Matlock, B.S. Howerton, D.A. Atwood, Irreversible precipitation of mercury and lead, Journal of Hazardous Materials 84 (2001) 73–82.
[13] J. Barron-Zambrano, S. Laborie, P. Viers, M. Rakib, G. Durand, Mercury removal and recovery from aqueous solutions by coupled complexation-ultrafiltration and electrolysis, Journal of Membrane Science 229 (2004) 179–186.
[14] T.S. Anirudhan, L. Divya, M. Ramachandran, Mercury(II) removal from aqueous solutions and wastewaters using a novel cation exchanger derived from coconut coir pith and its recovery, Journal of Hazardous Materials 157 (2008) 620–627.
[15] Z. Li, Q. Wei, R. Yuan, X. Zhou, H. Liu, H. Shan, Q. Song, A new room temperature ionic liquid 1-butyl-3-trimethylsilylimidazolium hexafluorophosphate as a solvent for extraction and preconcentration of mercury with determination by cold vapor atomic absorption spectrometry, Talanta 71 (2007) 68–72.
[16] Y. Terashima, H. Ozaki, M. Sekine, Removal of dissolved heavy metals by chemical coagulation, magnetic seeding and high gradient magnetic filtration, Water Research 20 (1986) 537–545.
[17] S Basha, Z.V.P. Murthy, B. Jha, Sorption of Hg(II) onto *Carica papaya*: experimental studies and design of batch sorber, Chemical Engineering Journal 147 (2009) 226–234.
[18] X. Liu, C. Qi, T. Bing, X. Cheng, D. Shangguan, Specific mercury(II) adsorption by thymine-based sorbent, Talanta 78 (2009) 253–258.
[19] I.B. Rae, S.W. Gibb, S. Lu, Biosorption of Hg from aqueous solutions by crab carapace, Journal of Hazardous Materials 164 (2009) 1601–1604.
[20] S. Manchester, X. Wang, I. Kulaots, Y. Gao, R.H. Hurt, High capacity mercury adsorption on freshly ozone-treated carbon surfaces, Carbon 46 (2008) 518–524.

[21] S. Wang, H. Wu, Environmental-benign utilisation of fly ash as low-cost adsorbents, Journal of Hazardous Materials 136 (2006) 482–501.
[22] M.A. López-Antón, P. Abad-Valle, M. Díaz-Somoano, I. Suárez-Ruiz, M.R. Martínez-Tarazona, The influence of carbon particle type in fly ashes on mercury adsorption, Fuel 88 (2009) 1194–1200.
[23] S.T. Chung, K.I. Kim, Y.R. Yun, Adsorption of elemental mercury vapor by impregnated activated carbon from a commercial respirator cartridge, Powder Technology 192 (2009) 47–53.
[24] J. Goel, K. Kadirvelu, C. Rajagopal, V.K. Garg, Removal of mercury(II) from aqueous solution by adsorption on carbon aerogel: response surface methodological approach, Carbon 43 (2005) 197–200.
[25] D.L. Guerra, R.R. Viana, C. Airoldi, Adsorption of mercury cation on chemically modified clay, Materials Research Bulletin 44 (2009) 485–491.
[26] L.A. Belyakova, O.M. Shvets, D.Y.e. Lyashenko, Formation of the nanostructure on a silica surface as mercury(II) ions adsorption sites, Inorganica Chimica Acta 362 (2009) 2222–2230.
[27] J. Aguado, J.M. Arsuaga, A. Arencibia, Influence of synthesis conditions on mercury adsorption capacity of propylthiol functionalized SBA-15 obtained by co-condensation, Microporous and Mesoporous Materials 109 (2008) 513–524.
[28] C.B. Lopes, M. Otero, Z. Lin, C.M. Silva, J. Rocha, E. Pereira, A.C. Duarte, Removal of Hg^{2+} ions from aqueous solution by ETS-4 microporous titanosilicate—kinetic and equilibrium studies, Chemical Engineering Journal 151 (2009) 247–254.
[29] X.-W. Wu, H.-W. Ma, J.-H. Li, J. Zhang, Z.-H. Li, The synthesis of mesoporous aluminosilicate using microcline for adsorption of mercury(II), Journal of Colloid and Interface Science 315 (2007) 555–561.
[30] E. Yavuz, B.F. Senkal, N. Bicak, Poly(acrylamide) grafts on spherical polyvinyl pyridine resin for removal of mercury from aqueous solutions, Reactive and Functional Polymers 65 (2005) 121–125.
[31] R. Akkaya, U. Ulusoy, Adsorptive features of chitosan entrapped in polyacrylamide hydrogel for Pb^{2+}, $UO_2{}^{2+}$, and Th^{4+}, Journal of Hazardous Materials 151 (2008) 380–388.
[32] S.H Jang, Y.G. Jeong, B.G. Min, W.S. Lyoo, S.C. Lee, Preparation and lead ion removal property of hydroxyapatite/polyacrylamide composite hydrogels, Journal of Hazardous Materials 159 (2008) 294–299.
[33] H. Kasgöz, S. Özgümüs, M. Orbay, Modified polyacrylamide hydrogels and their application in removal of heavy metal ions, Polymer 44 (2003) 1785–1793.
[34] C.J. Brinker, G.W. Scherer, Sol–Gel Science. The Physics and Chemistry of Sol–Gel Processing, Academic Press, New York, 1990.
[35] S.S. Kistler, Coherent expanded aerogels and jellies, Nature 127 (1931) 741.
[36] H. El Rassy, P. Buisson, B. Bouali, A. Perrard, A.C. Pierre, Surface characterization of silica aerogels with different proportions of hydrophobic groups, dried by the CO_2 supercritical method, Langmuir 19 (2003) 358–363.
[37] Z. Novak, M. Habulin, V. Krmelj, Z. Knez, Silica aerogels as supports for lipase catalyzed esterifications at sub- and supercritical conditions, The Journal of Supercritical Fluids 27 (2003) 169–178.
[38] C.A.M. Mulder, J.G. Van Lierop, Preparation, densification, characterization of autocalve dried SiO_2 gels, in: J. Fricke (Ed.), Aerogels, Springer Verlag, 1986, p. 68.
[39] H. Ramadan, T. Coradin, S. Masse, H. El-Rassy, Synthesis and characterization of mesoporous hybrid silica–polyacrylamide aerogels and xerogels, submitted for publication.
[40] S. Brunauer, P.H. Emmett, E. Teller, Adsorption of gases in multimolecular layers, Journal of the American Chemical Society 60 (1938) 309–319.
[41] E.P. Barrett, L.G. Joyner, P.P. Halenda, The determination of pore volume and area distributions in porous substances. I. Computations from nitrogen isotherms, Journal of the American Chemical Society 73 (1951) 373–380.
[42] Nomenclature, symbols, units and their usage in spectrochemical, analysis. II. Data interpretation analytical chemistry division, Spectrochimica Acta Part B: Atomic Spectroscopy 33 (1978) 241–245.
[43] S. Lowell, J.E. Shields, M.A. Thomas, M. Thommes, Characterization of Porous Solids and Powders: Surface Area, Pore Size, and Density, Kluwer Academic Publishers, Dordrecht, The Netherlands, 2004.
[44] G. Socrates, Infrared and Raman Characteristic Group frequencies: Tables and Charts, 3rd ed., John Wiley & Sons, 2001.
[45] A. Duran, J.M. Fernandez Navarro, P. Casariego, A. Joglar, Optical properties of glass coatings containing Fe and Co, Journal of Non-Crystalline Solids 82 (1986) 391–399.
[46] H. Gunzler, H.-U. Gremlich, IR Spectroscopy: An Introduction, Wiley-VCH, 2002.
[47] Y. Fan, M. Zhang, Y.-Q. Feng, Poly(acrylamide-vinylpyridine-N,N′-methylene bisacrylamide) monolithic capillary for in-tube solid-phase microextraction coupled to high performance liquid chromatography, Journal of Chromatography A 1099 (2005) 84–91.
[48] L.Z. Peng Liu, Zhixing Su, Core/shell SiO_x@PAM nanospheres from UV-assisted surface-initiated free radical polymerization, Journal of Applied Polymer Science 100 (2006) 3433–3438.
[49] R.J. Hunter, Zeta Potential in Colloid Science, Academic Press, New York, 1981.
[50] I. Langmuir, The adsorption of gases on plane surfaces of glass, mica and platinum, Journal of the American Chemical Society 40 (1918) 1361–1403.
[51] H. Freundlich, Of the adsorption of gases. Section II. Kinetics and energetics of gas adsorption. Introductory paper to section II, Transactions of the Faraday Society 28 (1932) 195–201.
[52] M.J. Tempkin, V. Pyzhev, Acta Physiochimica URSS 12 (1940) 217–222.
[53] M.M. Dubinin, L.V. Radushkevich, Equation of the characteristic curve of activated charcoal, Chem. Zentr. 1 (1947) 875.
[54] D.D. Duong, Adsorption Analysis: Equilibria and Kinetics, Imperial College Press, London, 1998.
[55] Y.S. Ho, G. McKay, Pseudo-second order model for sorption processes, Process Biochemistry 34 (1999) 451–465.
[56] Z. Aksu, A.I. TatlI, Ö. Tunç, A comparative adsorption/biosorption study of Acid Blue 161: effect of temperature on equilibrium and kinetic parameters, Chemical Engineering Journal 142 (2008) 23–39.
[57] M. Sarkar, P.K. Acharya, B. Bhattacharya, Modeling the adsorption kinetics of some priority organic pollutants in water from diffusion and activation energy parameters, Journal of Colloid and Interface Science 266 (2003) 28–32.
[58] W.J. Weber, J.C. Morriss, Kinetics of adsorption on carbon from solution, Journal of the Sanitary Engineering Division 89 (1963) 31–60.
[59] L. Abramian, H. El-Rassy, Adsorption kinetics and thermodynamics of azo-dye Orange II onto highly porous titania aerogel, Chemical Engineering Journal 150 (2009) 403–410.